Chapter III

Influence of dopants and γ-irradiation on radiative events of Eu^{3+}:Gd_2O_3 nanosystems

Radiation exposure has a profound effect on the optical, electrical and physical properties of materials, and to the extent which primarily depends on the doses used [1]. The degree of crystallinity and aligned orientation can be introduced at high enough doses of radiation. In our study, the GNP nanopowder was first dispersed in millipore water® and then subjected to gamma irradiation. Upon γ -ray irradiation of liquids, most of the energy is absorbed by water, and so water radiolysis might take place, which results in formation of reactive species such as oxidizing hydroxyl radical (OH^-) and very powerful reducing radicals. The interaction generates free radicals by radiolysis process which recombine or interact with other species present in the solution and alter optical properties. High energetic γ - irradiation is also capable of creating and annihilating point defects in chemically stable Gd_2O_3 system [2, 3]. With the aim and motive to probe and associate the ED and MD transitions involved in Eu, a thorough analysis of photoluminescence aspects has been considered in this chapter.

3.1. Identifying relevant D-F transitions in the PL spectra of the RE doped Gd_2O_3 nanosystem

The room temperature steady state PL excitation (PLE) as well as PL emission spectra for both the undoped and Eu-doped GNP can be found in **FIGURE 3.1**.The excitation spectra of doped GNP (λ_{em}=612 nm) displayed a small broad peak at ~230 nm, attributed to CTB and a highly intense band centring at ~256 nm, known to result in intense emission from the $^5D_0$ levels of Eu^{3+} (inset of **FIGURE 3 (B)(a)** [4]. The PL excitation spectra also revealed the CTB observed in the absorbance profiles. It is known that the Eu^{3+} ions are first excited to higher $^5D_{1,2,3}$ levels and then relaxed non-radiatively by multiphonon emission to populate $^5D_0$ level [5]. Moreover, a widely accepted excitation mechanism for the RE ions displaying PL can also account for where with the incomplete inner shells. It is known that the introduction of dopant Eu^{3+} can lead to generation of deep defects *i.e.* deep levels positioned close to the middle of the band gap. These defects are responsible for non-radiative recombination of electrons and holes. Since the dopant and host have isoelectronic character (same

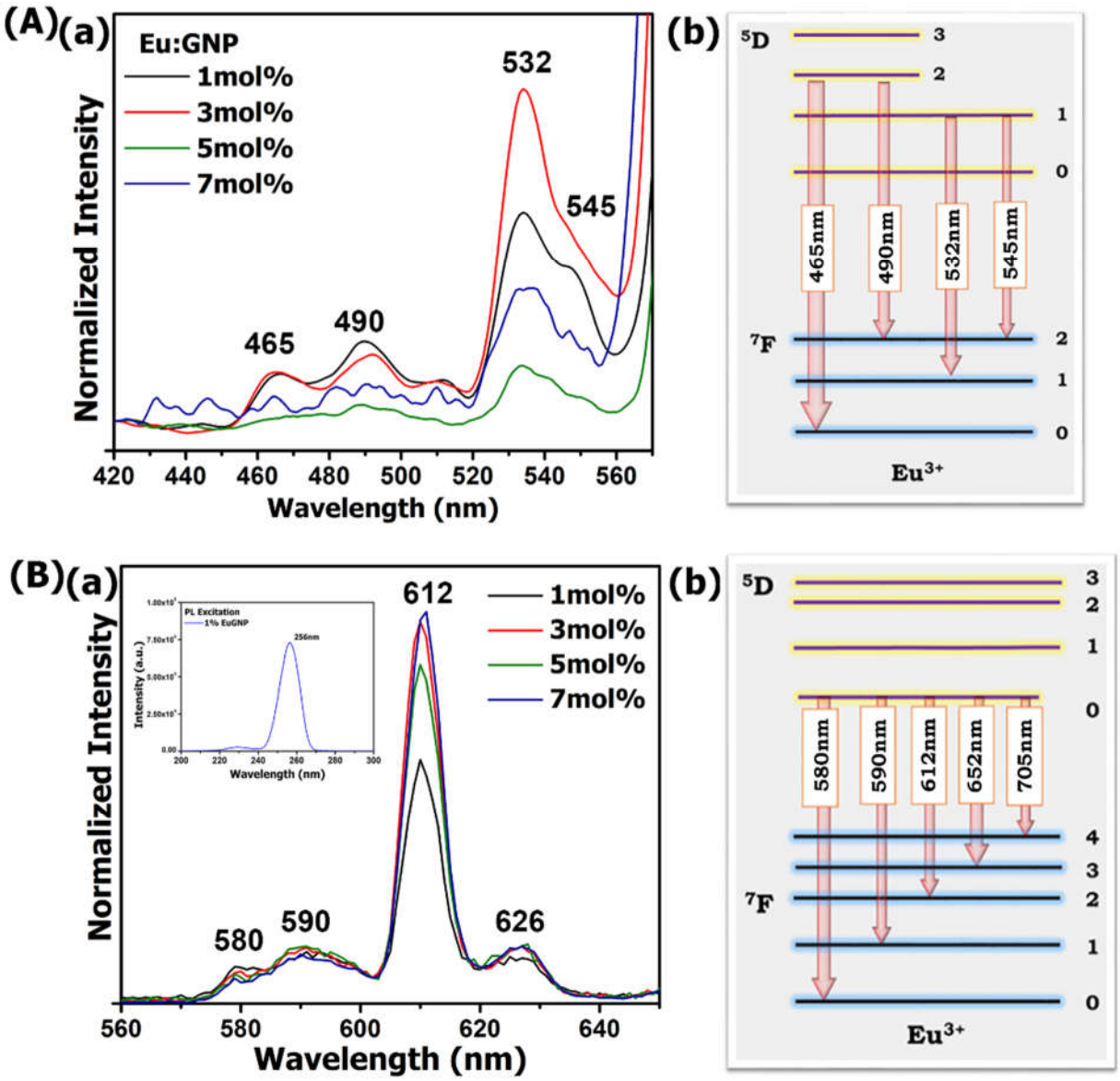

FIGURE 3.1. PL emission profiles in the (A)(a) blue-green regime, (B)(a) orange-red regime for the doped samples**.** The PLE spectra for EuGNP is provided as inset of (B)(a) and schematic diagram of involved energy levels corresponding to transitions observed in the (A)(b) blue-green region and B(b) orange red region are shown in (B)(b).

overall charge and appear to be neutral with respect to the host), part of recombination energy can be transferred to the matrix levels, thereby promoting it to an excited state [6].

The mechanism of excitation or population of $^5D_0$ level of Eu^{3+} in Gd_2O_3 host matrix is via the energy transfer from the trap-levels (defect states of the matrix host

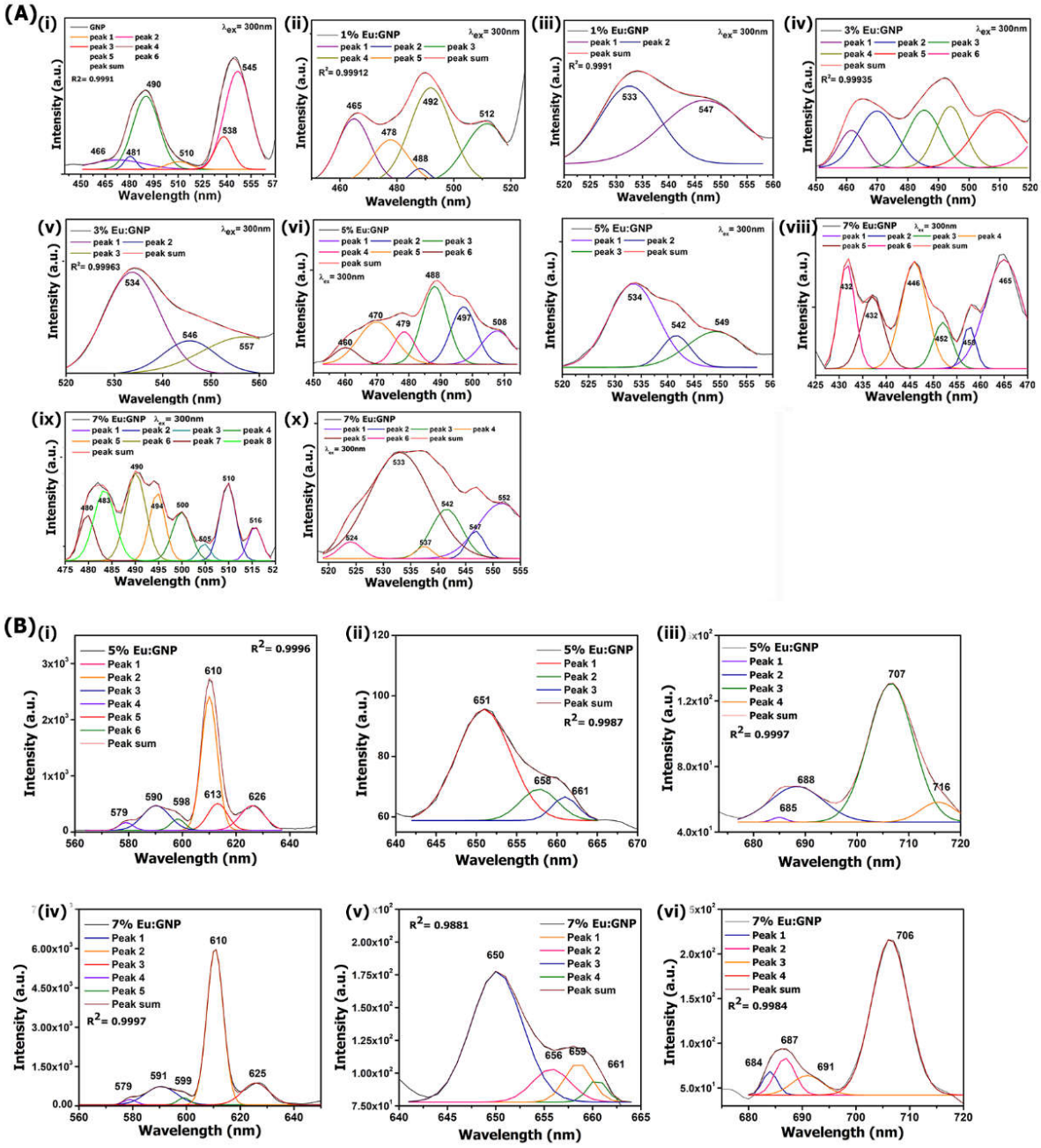

FIGURE 3.2. Deconvolved PL emission profiles in the (A) blue green regime with 300nm excitation wavelength for (i) GNP, (ii,iii) 1% EuGNP, (iv,v) 3% EuGNP, (vi,vii) 5% EuGNP and (viii-x) 7% EuGNP; and in the (B) orange red regime with 400nm excitation for 5% EuGNP (i-iii) and 7% EuGNP (iv-vi).

ions, Gd^{3+}) to that of the activator ions. In order to excite the ions to the higher levels, the system was excited at 300 nm and the emission spectra were observed in the blue-

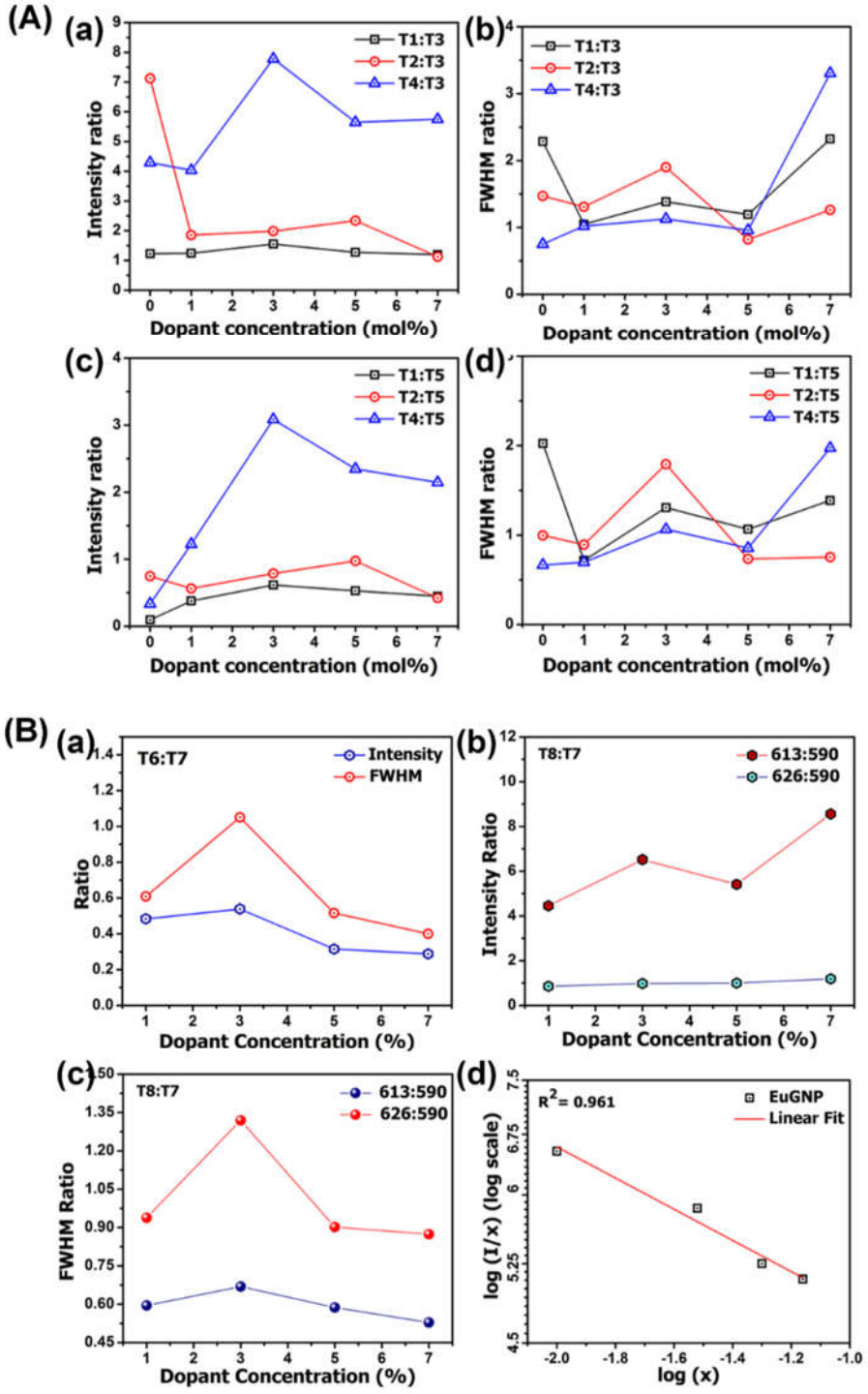

FIGURE 3.3. Intensity and FWHM ratios for the various assigned PL emission peaks in (A) blue green regime and (B) orange-red regime. B(d) displays the plot according to Dexter's model following Eqn. 6 for the various doped samples

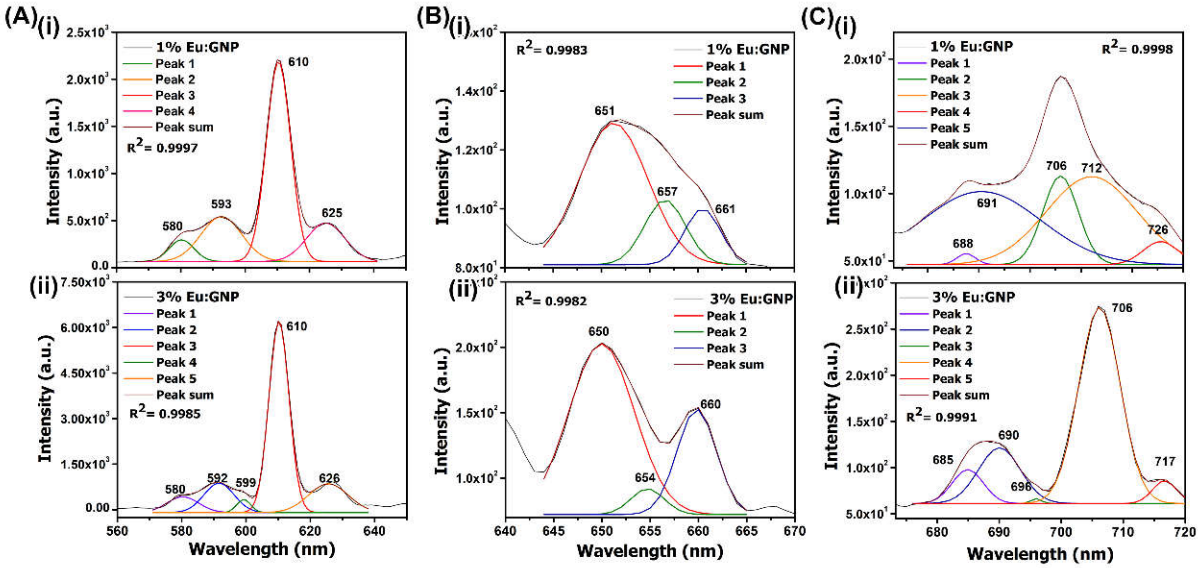

FIGURE 3.4 Deconvolved PL emission profiles in the orange-red regime with 400 nm excitation wavelength displaying emissions *viz.* (A) $^5D_0$-$^7F_{0,1,2}$ (B) $^5D_0$-$^7F_3$ (C) $^5D_0$-$^7F_4$ for (i) 1% EuGNP and (ii) 3% EuGNP respectively.

green regime. Excitation at 300 nm has led the undoped Gd_2O_3 displaying two prominent peaks in the blue-green region, centred at 490 nm and 545 nm (**FIGURE 3.2 (a)).**

As for the undoped samples, the observed peak at 490 nm is originated mainly due to Schottky and Frenkel defect types which arise due to thermal lattice disordering as a consequence of interstitial Gd^{3+} ions. While the other peak at 545 nm peak is due to the co-localization of electrons in the Stark level transitions from ^6G_J state of Gd^{3+}[3]. The 538 nm peak observed can be attributed to excitation corresponding to $^8S_{7/2}$ to ^6I_J optical transitions in Gd^{3+} **(FIGURE 3.2(A)(a))** [7]. The host lattice can henceforth be considered as vacancy type luminescent active system. On the other hand, the doped samples displayed distinctive transitions in blue-green regime as evident in **FIGURE 3.1 A(b).**

In order to acquire a thorough evaluation and a better perspective at large, the asymmetric PL spectra were deconvolved considering the normalized multi-peak Gaussian fitting. The condition was to match experimental curve with the empirical curve, later being emerged as consequence of superposition of deconvolved parts.

With a good statistical agreement such a fitting enables us to identify the peak positions and compare intensities as well as FWHM at large. Upon deconvolution, the peak centres were found to be located at ~ 465 nm, 490 nm, 512 nm, 532 nm and 545 nm, attributing to the $^5D_2 \rightarrow {}^7F_0$, $^5D_2 \rightarrow {}^7F_2$, $^5D_2 \rightarrow {}^7F_1$, $^5D_1 \rightarrow {}^7F_1$, and $^5D_1 \rightarrow {}^7F_2$ transitions in Eu^{3+}; respectively [8, 9]. For convenience, these transitions are annotated as, *T*1, *T*2, *T*3, *T*4, and *T*5; respectively **(FIGURE 3.2. (A)(b-j))**. These transitions are complicated given that a large number of crystal field transitions influence these levels and are rarely reported. The observations indicate inhibition of non-radiative transitions between $^5D_1$ to $^5D_0$, typical for temperatures below 200 K, and leads to non-equilibrium back

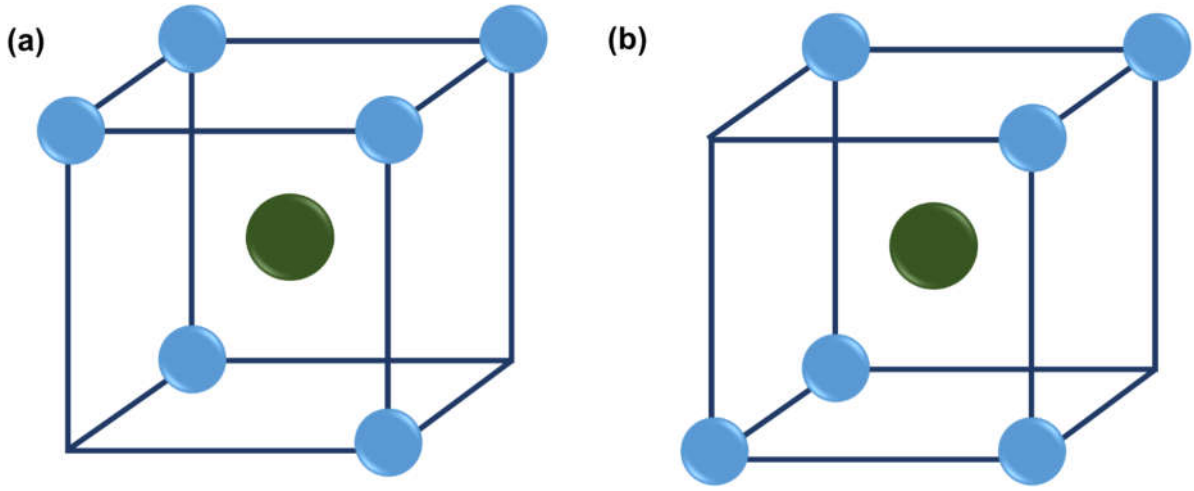

FIGURE 3.5 Schematic illustration for atomic positioning for (a) C_2 site and (b) S_6 site symmetry (green dot- central atom, blue dot- neighboring atoms)

up of population in $^5D_1$ level [5]. Based on the selection rules which are strictly valid in the Russel Saunders coupling scheme, these transitions are termed- electrically driven (ED) (*T*1, *T*2, *T*4) or magnetically driven (MD) (*T*3 and *T*5). Here, *T*4 is the most intense emission and is found to be maximum for 3% EuGNP **(FIGURE. 3.1 A(a), 3.2 A(c))**. The T2/T5 full width becomes maximum for 3% EuGNP as can be found in **FIGURE 3.3 A(d)**.

In general, above bandgap excitation wavelength facilitates nearby carrier trapping site before reaching the dopant ions; hence 400 nm was also chosen as the wavelength of excitation [10]. The PL emission profiles in the red regimes were then

revealed. Various transitions via $^5D_0 \rightarrow {}^7F_J$ (J=0,1,2,3,4) in the red and far-red regime are witnessed with intensities far greater than that from the higher excited levels **(FIGURE 3.1 B(a,b)).** For clarity, these transitions are annotated as T6, T7, T8, T9, T10; respectively. Typically, ^7F_J, J=0,2,4 (T6, T8, T10) are accompanied by ED transitions; while J=1,3 (T7, T9) represent MD transitions. In a compound where Eu^{3+} ion occupies no centre of symmetry at all, both ED and MD transitions are possible. The J=0,3,5 level also display J mixing with other sublevels of J=2,4.

Strikingly, upon deconvolution, we observe the presence of very rarely reported T6 ($^5D_0$-$^7F_0$ transition), positioned at ~580 nm which is ordinarily forbidden according to the Laporte's rule and can be found from **FIGURE 3.4.** [11]. Observance of forbidden T6 transition is explained by many researchers on the basis of J-mixing due to the crystal field perturbation or mixing of low lying charge transfer states into wave-functions of $4f^6$ configuration [12-15]. Not surprisingly, we observe the intensity of T6 to be half to that of T7, for the 3% EuGNP specimen (Figure 3.3)). The intensity distribution of the transitions among different $^5D_0 \rightarrow {}^7F_J$ (J = 0, 1, 2, 3) levels are dependent on the local symmetry of the dopant ions and can be described in terms of Judd–Ofelt theory [16, 17]. As witnessed, T7 is a strong MD transition and is largely independent of the Eu ion environment unlike T8, which is a hypersensitive transition. [18]. Depending on the chemical environment of the ions, the shape of the spectra may differ appropriately with a change in the relative intensity as well as crystal field splitting of the bands. The ED transitions are known to be hypersensitive in nature i.e., its emission profile may alter with the local symmetry around the luminescent centres. The nonlinear variation in PL intensity witnessed with increasing doping levels would suggest that the Eu_2O_3 phases are not formed separately [19].

Although rarely discussed, reports suggest that the intensity of the forbidden transitions can be comparable with that of T7 feature [20]. The intensity ratio decreases upon increasing doping levels representing possible alterations in site-symmetry. The single peak for T6 arises due to a non- degeneracy of the involved levels and single site as well as species [21, 22]. Yet again, as predicted earlier, the origin of ~580 nm peak indicates that fraction of Eu^{3+} ions occupy C_{nv}, C_n or C_s symmetry [11]. Another

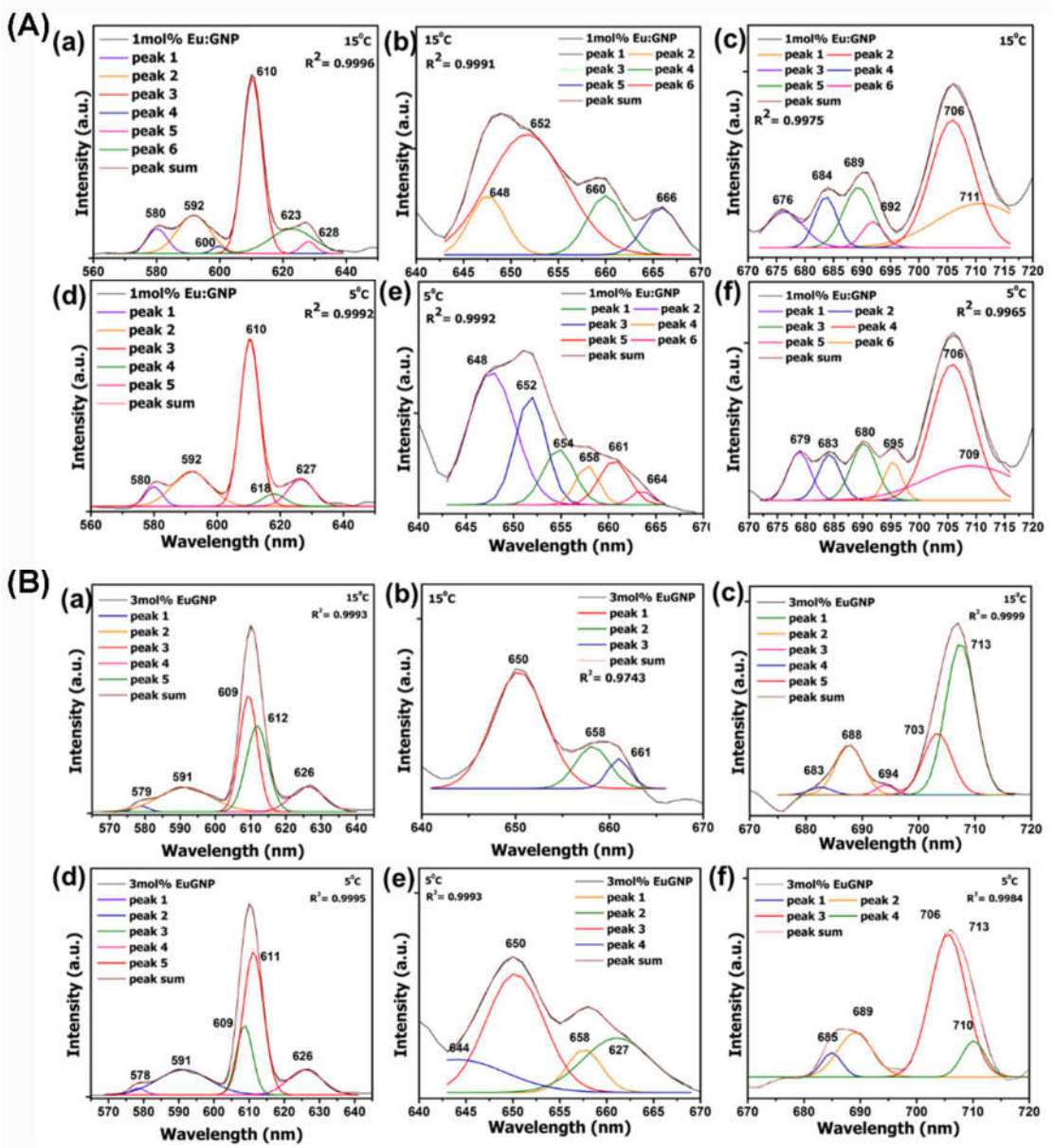

FIGURE 3.6. Temperature dependent PL emission profiling of the samples doped below quenching concentration for (A) 1% EuGNP and (B) 3% EuGNP, studied at 15 °C as shown in (a-c) and 5 °C as shown in (d-f).

important observation is broad *T*6 profiles with FWHM ratio of *T*6 and *T*7 being highest for 3%Eu:GNP **(FIGURE 3.3 B(i))** which indicates that Eu^{3+} ions occupy the S_6 sites (while broad *T*8 signifies occupation in C_2 sites) [11]. The dopants in cubic phase Gd_2O_3 are allowed to reside randomly in cation sites with either of the two symmetries- C_2 (24 non-centrosymmetric sites) and S_6 (8 centrosymmetric sites) (**FIGURE 3.5**) [23, 24]. For Eu^{3+} ions occupying the S_6 site, only the MD will be

observed on the other hand under C_2 site symmetry Stark splittings are realised [25]**.** Only 11% of the total emission intensity is from the excited Eu^{3+} ions that occupy S_6 site [26]. Our observations with both MD and ED transitions make it clear that dopant ions (Eu^{3+}) reside in both the C_2 as well as S_6 sites [27]. The occurrence of ED *T*8 depicts that the Eu^{3+} ions are incorporated away from the centrosymmetric site (**FIGURE 3.4(a))** [28]. The *T*7 and *T*8 peak splitting with additional peak centering ~ 599 nm (absent in 1% Eu:GNP) is observed along with strongly intense emission for *T*8 centring at ~626 nm which indicates that lower doping levels have proper cubic crystal field and the site symmetry is compromised in higher doping levels [29]. Our XPS based observations also suggested better interaction between the orbitals at lower concentrations as discussed in Chapter II.

To be mentioned, close temperature dependent emission profiles are examined at two distinct temperatures (5 ˚C and 15 ˚C), for 1% and 3% doping levels (**FIGURE 3.6**). While comparing, higher doping levels were not considered, as they suffer from concentration quenching effect. Interestingly, upon lowering the temperature to 5˚C the intensity of ~612 nm peak in 1% EuGNP is enhanced, while the response of 3% EuGNP remains constant. The peak splitting was seen to be more prominent for *T*9 as well as *T*10. The vibronic intensity of *T*8 is known to be suppressed at lower temperatures and consequently, sharper profiles were observed [30]. The splitting of ~626 nm peak with the occurrence of peaks at ~623 nm and ~628 nm at 15 ˚C has been witnessed **(FIGURE 3.6 A(a)).** Remarkably, the Eu^{3+} transitions were known to split with a degeneracy of (*J*+1). At a temperature of 5˚C, the peaks appear at ~618 nm and ~627 nm. Thus with a moderate change in temperature, a pronounced effect with occurrence of a peak at ~609 nm, is possibly due to a splitting of most intense peak in the spectra at ~612 nm. The proportionate change in vibronic response may account for such an effect, and noticeable for doping levels below critical concentration.

Since the vibronic intensity of *T*8 is known to be lowered at low temperatures, we also studied the PL response for the system at below room temperature conditions. Strikingly, a clear peak splitting is evident for the (ED) transitions to $^7F_2$ as the temperature was lowered. The $^7F_2$ has four levels, three non-degenerate and one

degenerate and speaking in terms of polarization of light, the perpendicular component leads to peak centering at 619.3 nm (non-degenerate), while component polarized along *c*-axis at 615.5 nm (degenerate). As far as the splitting of 650 nm peak of *T*9 is concerned, $^7F_3$ has three non-degenerate and two doubly degenerate states. The peaks at 650 nm has optically active components and those at 654 nm and 656 nm are due to components perpendicular to c-axis. The peak observed at 652 nm is due to the component parallel to *c*-axis. The peak around 648 nm is involved with higher state transitions [31].

3.2. Concentration quenching effect with dopant variation

We observed luminescence quenching to occur beyond the level of critical doping (~ 3% Eu:GNP). The intensity ratio of the most prominent ED transition (*T*8) to MD transition (*T*7) is found to be maximum for the highest doping concentration (7% EuGNP), but the peak is found to be sharper than that for 3% EuGNP. The ratio being as high as 9 times to that of MD T7 being common and can be found in earlier reports [32, 33]. An observable increase in intensity for the 7% doped Eu:GNP system beyond critical concentration can be elucidated considering that higher doping concentrations favour emission from $^5D_0$ level at the expense of higher excited states related transitions and hence the T8 intensity shoots up. The quenching in high energy level emission could be favourable for lower energy emission following multiple cross relaxation events [34] viz.,

$$^5D_1\,(Eu^{3+}) + {}^7F_0\,(Eu^{3+}) \rightarrow {}^5D_0\,(Eu^{3+}) + {}^7F_3\,(Eu^{3+}) \qquad (4)$$

Concentration quenching is mainly due to the transfer of excitation energy from an activator to another so that the energy is lost radiationlessly [35]. It is noteworthy that non-uniform incorporation of Eu^{3+} ions throughout the lattice possibly increases with increasing concentrations which leads to Eu^{3+} cluster zones and zones barren of Eu^{3+} ions as well. Therefore, the Eu^{3+} dopants experience a variety of local environments for higher doping cases leading to altered local field and asymmetry induced splitting [36]. The distance between nearest neighbours

(activators) also plays a decisive role in quenching. The critical distance R_c for the critical concentration X_c= 3 mol% was determined to be ~1.36 Å using the following equation otherwise known as Blasse's energy transfer equation: [37, 38]

$$R_C = \left(\frac{3V}{4\pi N X_c}\right)^{\frac{1}{3}}, \quad (5)$$

where, 'N' (=32) is number of cations per unit cell for Gd_2O_3 and 'V' is the unit cell volume determined using '*Powder cell for Windows®*' to be 1268.48 $Å^3$. The sudden rise in intensity for 7% EuGNP can also be explained considering a change in Coulomb force of dopants upon higher doping level, which allows Eu^{3+} ions to experience different crystal field and consequently occupy non-centrosymmetric sites [39].

For concentrations beyond critical, most of the activators have other activators as nearest neighbours and hence the phonon spectrum and lattice constants changes and the probability of thermal quenching varies. The nature of the concentration quenching mechanism of Eu^{3+} can be determined following Dexter theory: [21, 40]

$$I \propto x\left[1 + \beta(x)^{\frac{s}{3}}\right]^{-1} \quad (6)$$

In equation, s= 3,6,8,10 depends on the series of electronic multipole interaction and is a decisive factor the value of which indicates the type of interaction involved, 'β' is a constant [41]**.** 's' can duly be determined plotting log (I/x) vs log x on a logarithmic scale of I/x. In our study, $s/3$ = 1.32, i.e. s = 3.96 **FIGURE 3.3(B)(d).** This value, s~3 corresponds to the exchange interaction of ions to be the prime mechanism behind the quenching. Interestingly, in our case, the effectual contribution of exchange interaction on splitting of Gd*4d* XPS signals was profoundly observed. Overlapping of near zone ED fields of activators occur between activators and at sufficiently low concentrations only a small quanta of energy is quenched. Such an exchange interaction between ions occur when the ions are located near one another such that there is a sufficient overlap in their wave functions along with the coupling of spins

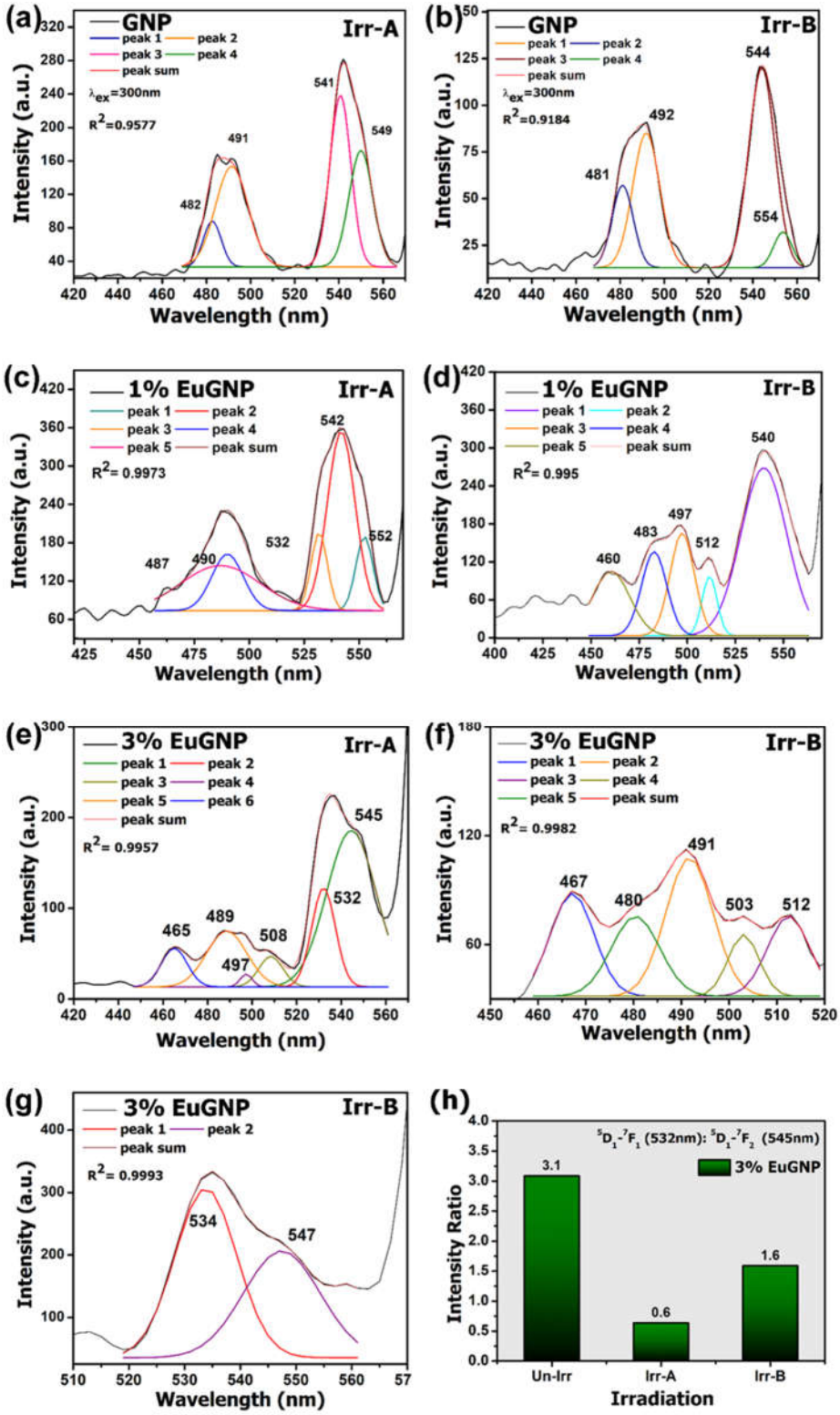

FIGURE 3.7. (a-g) PL emission profiles of as-prepared samples following gamma irradiation at varying doses observed in the blue green regime; (h) effect of irradiation on the intense ED and MD transitions displayed in a comprehensive manner in form of histogram for 3% EuGNP in the blue green regime

[42, 43]. Such an observation in red phosphor Eu:GNP is extremely crucial not only because of fundamental reasons but also its relevance in spin injection and transport.

3.3. Effect of γ-irradiation on steady state and time-resolved photoluminescence features

The deconvolved emission profiles for the irradiated samples are shown in **FIGURE 3.7** for the blue green regime and in **FIGURE 3.8** for the orange-red regime. The luminescence responses for both 1% and 3% doped samples as observed in the 450-550 nm range arising from higher energy levels-based transitions were found to be augmented. We are not aware of any known reports elaborating the effects of γ - irradiation in the blue-green region. During exposure, owing to interaction of γ - photon with the medium, electrons are emitted due to the Compton effect. These electrons can also be accommodated in pre-existing oxygen vacancies. As a consequence, adequate F^+ centres are formed. that are responsible for increased luminescence Usually, an energy transfer between Gd^{3+} and the F^{2+} centres leads to indirect pairing with excited state and subsequent radiative transition to ground state can occur thereby augmenting the luminescence [7].

Newer peaks are visible after irradiation that are ascribed to the defect formations due to radiation exposure. The important ED transition in this range centred at 532 nm is found to gain intensity (three-fold) after irradiation. As for the FWHM ratio of ED and MD transition in the red regime, we observe an irradiation dosage dependent improvement for both 1% and 3% doping levels. We can thus be ascertained that irradiation has induced creation of closely packed non-radiative trap centres which include both neutral as well as ionized vacancies.

In reference to un-irradiated system, as for the 1% EuGNP initially at Irr-A (0.8 KGy), the intensity ratio *T*8:*T*7 decreased and then increased to regain a comparable value upon subjected to Irr-B (2.4 kGy). Conversely, in 3% EuGNP the intensity ratio *T*8:*T*7 increases for irr-A but declines at the higher dose, irr-B as depicted in **FIGURE 3.7**.

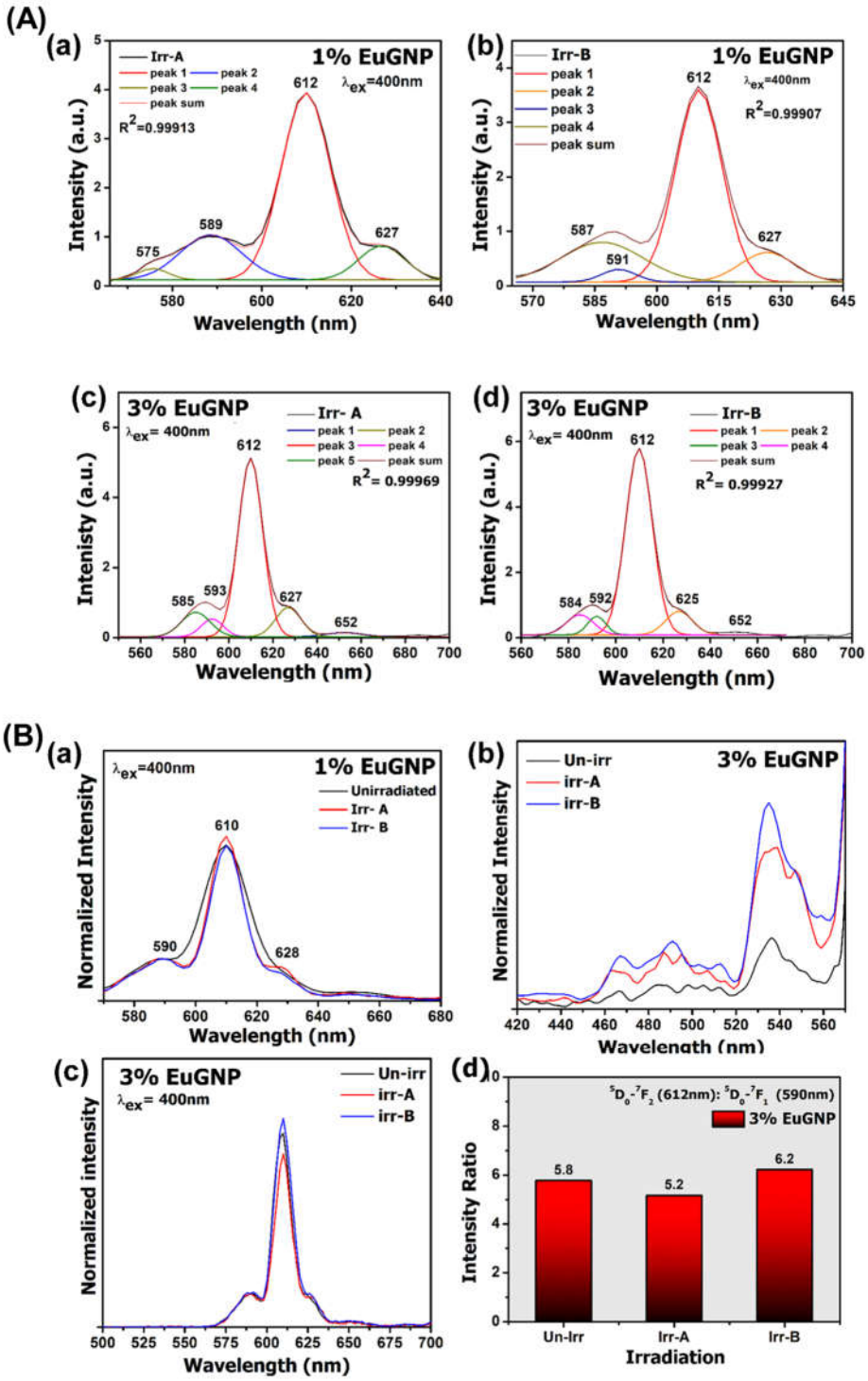

FIGURE 3.8. PL emission profiles observed in the orange red regime for γ-irradiated (A) 1% EuGNP and (B) 3% EuGNP. Comparative plot for the effect of irradiation on the intense ED and MD transitions is displayed for 1% EuGNP in (B) (a) and for 3% EuGNP in (B) (b) & (c). A comprehensive histogram illustrating the intensity ratio for the important ED and MD transition in the orange red regime.for 3% EuGNP can be found in (B) (d)

MD transitions ~590 nm (and ~585 nm) after irradiation impact. In all cases we observed that the build-up phase did not begin from zero indicating possibility of two excitation pathways to populate the $^5D_0$ level, one being via $^5D_1$ level and the other promoting ions directly into $^5D_0$ [5].

In order to obtain further insight into the species excited state dynamics, and its relevance with dose dependency, TR-PL analysis has been performed. In all cases we observed that the build-up phase did not begin from zero indicating possibility of two excitation pathways to populate the $^5D_0$ level, one being via $^5D_1$ level and the other promoting ions directly into $^5D_0$ (**FIGURE 3.9**)[5]. Almost all of the emission peaks featured decay profiles that were single exponential. Lifetime is reported to be 1 ms for C_2 site emission while for Eu^{3+} ions in S_6 sites the life-time increases by at least three-fold (~3-4 ms) [4, 27, 44]. The lowering in lifetimes, upon increasing doping concentration is attributed to an increase in non-radiative relaxation caused by the surface defects acting as quenchers [45]. In this regard, a very limited literature was devoted to determining the decay parameters of the transitions in the blue –green regime.

In order to determine the decay lifetime, all curves were primarily fitted to a single exponential function using *Origin 8.5*®. Interestingly, a steep decrease has been realized for the lifetimes of peaks centred at ~490 nm and 545 nm, upon doping. In our study, we observed the lifetime of *T*8 to be ~1.6 ms for 1% EuGNP and ~1.4 ms for 3% EuGNP. These transitions are dominated over by the strong *D-F* transitions upon Eu^{3+} doping, thereby changing the decay dynamics of the peaks. The effect of irradiation can be observed to induce impacts for both the doping levels, where the lifetime drops for Irr-A and again regains its value for Irr-B in case of 590 nm and 626 nm emission lines. As for 613 nm, the lifetime of both 1% and 3% doped levels gets lowered upon irradiation and gained equal values. The lifetimes associated with MD transitions at ~590 nm, ~613 nm and ~626 nm followed similar trends upon varying doping levels. The lifetime of the both strongest MD and ED transitions drops substantially upon increasing the doping levels (up to 3%). However, the lifetime of

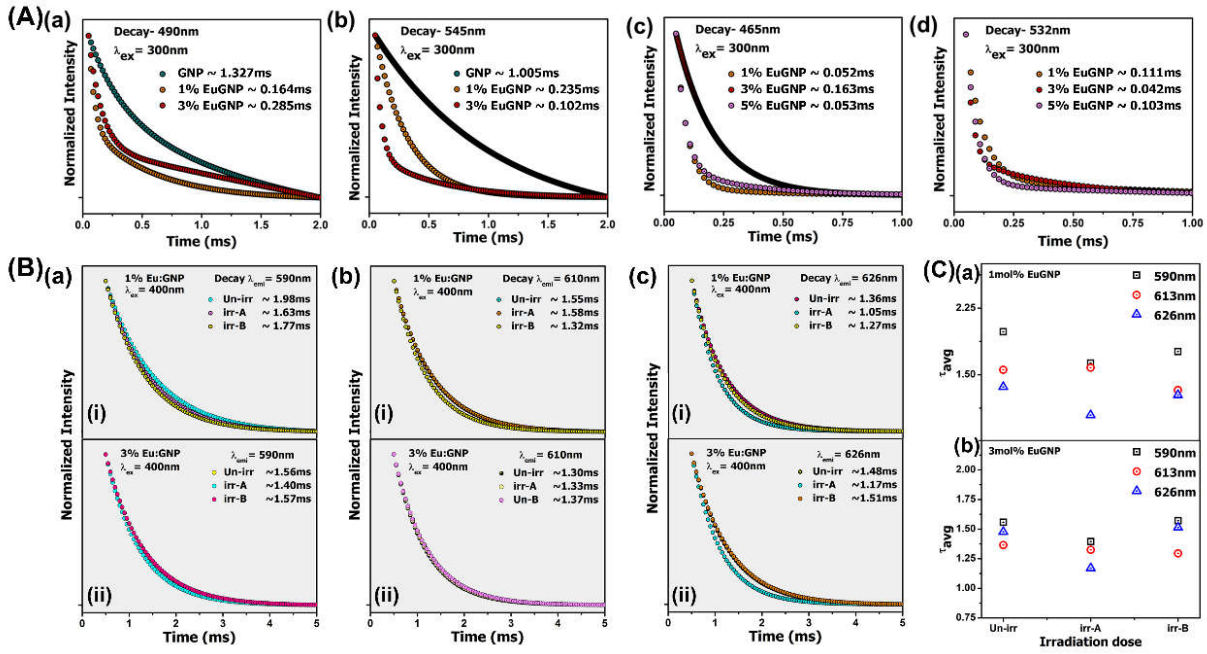

FIGURE 3.9. (A) TR-PL decay dynamics upon γ-irradiation for various transitions observed in (A) (a-d) blue-green region and (B) (a-c) orange-red region. (C) The effect of γ-irradiation on the average lifetime of the prominent *D-F* transitions in the orange-red regime.

~626 nm peak increased by ~0.12 ms upon increasing the dopant concentration from 1 mol% to 3 mol%. This incongruity with variation in lifetime of other peaks can be defined considering this peak arises from the splitting due to crystal field and since for a higher doping level the field is stronger and hence the transition has a different recombination route as compared to the other two transitions.

In the orange red regime, with increasing irradiation dose we observed a nonlinear variation in the intensity ratio for *T*8:*T*7. Nevertheless, for the lower dose the ratio drops but gets augmented as the dose was increased. The track interaction model (TIM) suggests localised entity as the electron-hole doubly occupied spatially correlated trap centre/luminescent centre pairs. For lower doses, number of generated luminescent / trap centres would be small which may not contribute to extra PL. We believe that at a relatively higher dose, formation of such localized entities would be greater as a result of which the spacing between them tends to decline. More importantly, the contribution to extra PL intensity would increase as observed in our case for higher doses.

Irradiation based experiments induce dislocations of activator ions to interact with the defect centres and hence complex multifaceted decay dynamics is expected. Effect of irradiation can be observed to have equally impacted both the doping levels, where the lifetime drops for irr-A and again regains its value for irr-B in case of 590 nm and 626 nm. Strikingly, for 613 nm the lifetime of both 1% and 3% doped levels dropped upon irr-B and gained equal values.

3.4. Manifested luminescence features upon inclusion of co-dopants (Na^+, K^+)

The room temperature PL emission spectra of the as-prepared Gd_2O_3:Eu^{3+} nanosystems co-doped with Na^+ and K^+ ions are mainly depicted in the orange-red regime, in **FIGURE. 3.10 (a)(i-vi)**. We do not observe any changes in the overall profile of the spectra upon inclusion of co-dopants into the system. The most intense ED and MD transitions maintained their positions in the spectra with relatively weak subsidiary peak at ~626 nm is due to the splitting of the ~612 nm transition. Here also, we witnessed the ED based $^5D_0 \rightarrow {}^7F_0$ transitions positioned at, ~580 nm. The effect of co-doping generally accounts for enhancing the PL response, as can be found in **FIGURE 3.11 (a,b).**

The EuGNP system offers a greater augmentation in the emission with K^+ co-doping as compared to its Na^+ co-doping counterpart, or simply without co-doping. We further analyzed the intensity of the ED transition (~612 nm, red emission) relative to the MD transition (~590 nm, orange emission), shown in **FIGURE. 3.11 (c)** and **TABLE 3.1.** It clearly shows that the ED- to- MD intensity ratio is relatively higher for the nanorod system (EuGNR) than for the nanoparticles (EuGNP), and without co-doping case. When codoped with either Na^+, or K^+, it was EuGNP which gave a stronger feature. Observably, the intensity ratio rises from ~2.9 for EuGNP to nearly four times upon co-doping with the alkali ions. Conversely, the EuGNR system exhibits a value of ~3.67 which enhances only slightly up to 3.74 with the inclusion of co-dopant K^+ into the EuGNR system (Fig. 3.10(c)). Interestingly, upon co-doping with Na^+, the intensity ratio gets lowered to ~3.5. Fig. 3.10(d) displays the schematic representation of underlying mechanisms such as energy sensitization and energy transfer between the involved dopant and co-dopants, leading to apparent

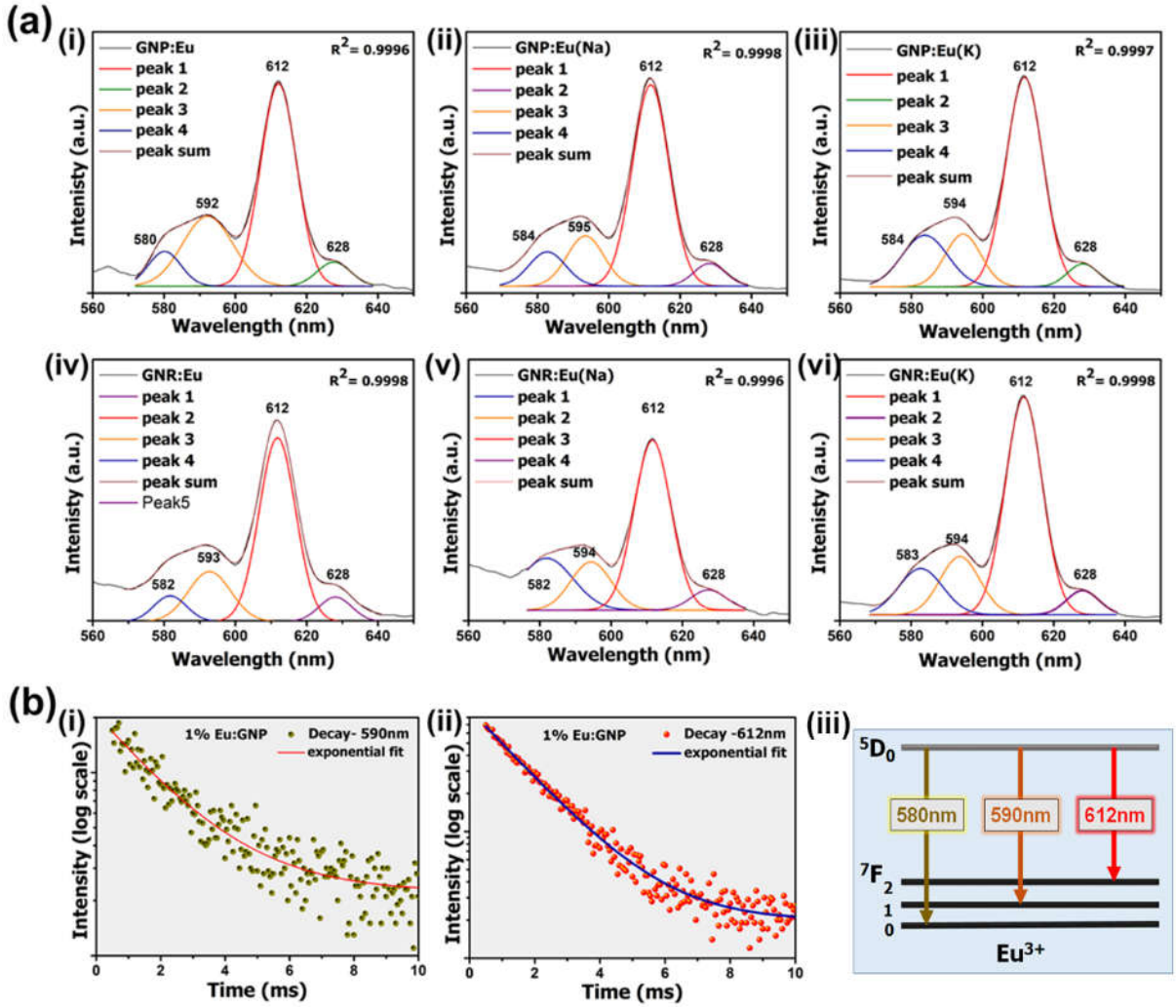

FIGURE 3.10: (a) De-convoluted photoluminescence spectra of (i) EuGNP, (ii) EuGNP(Na), (iii) EuGNP(K), (iv) EuGNR, (v) EuGNR(Na), and (vi) EuGNR(K) nanosystems. (b) TR-PL decay curves for 1% EuGNP system corresponding to emission peak (i) ~590 nm, and (ii) ~612nm. A schematic of important transitions is illustrated in (iii).

augmentation of luminescence discussed in later sections. We have also compared the subsidiary E D ($^5D_0 \rightarrow {}^7F_2$), ~626 nm peak with the MD ($^5D_0 \rightarrow {}^7F_1$), ~590 nm peak, and observed a rise in case of the co-doped EuGNP (Fig. 3.11 (a)). But a steady fall has been realized in case of the co-doped EuGNR (Fig. 3.11 (b)). This anomalous observation is discussed in the successive sections.

TABLE 3.1: Relative intensity ratios for various $D_0 \rightarrow F_j$ (j= 0,1 and 2) transitions for doped and co-doped Gd_2O_3 nanosystems

Samples	Ratio	Relative intensity		
		Eu only	Eu with Na	Eu with K
GNP	613-580 nm	5.83	5.87	4.06
	613-590 nm	2.90	4.01	3.98
	626-590 nm	0.35	0.45	0.44
	590-580 nm	0.49	0.42	0.42
GNR	613-580 nm	7.12	3.27	4.71
	613-590 nm	3.67	3.53	3.74
	626-590 nm	1.94	0.93	1.26
	590-580 nm	2.01	1.47	1.02

3.4.1. Effect of co-doping on local symmetry

As discussed earlier, Eu^{3+} ions occupying the sites with inversion centers reveal intense $^5D_0 \rightarrow {}^7F_1$ transition peaks while the $^5D_0 \rightarrow {}^7F_2$ transition remains parity forbidden. Hence, for intense red emission ($^5D_0 \rightarrow {}^7F_2$), it is required that the Eu^{3+} ions are located away from the inversion center and in addition, their local symmetry be distorted. Know that here intensity describes the number of transitional events occurring in each transition while FWHM is linked with their line broadening aspect.

Upon co-doping, the intensity ratio as well as FWHM ratio of 590 nm peak ($^5D_0 \rightarrow {}^7F_1$)- to-580 nm peak ($^5D_0 \rightarrow {}^7F_0$) would drop substantially (**FIGURE 3.12 (a,b)).** It is important to note that the intensity of MD transition (~590 nm) is insensitive to the changes in local symmetry of dopants and the observation suggests that the 580 nm peak has been broadened. Notably, the intensity and the FWHM of the peak positioned at ~580 nm defines the amount of Eu^{3+} ions occupying C_{nv}, C_n, or C_s symmetry [11]**.** Also, in **FIGURE. 3.12 (a),** we observe a decrement in intensity ratio between the ~612 nm and ~580 peak. This in turn suggests that as the co-doping led occupation in C_2 sites tends to rise, it results in a more intense ~580 nm peak noticeably. Apparently, GNPs derived via citrate gel route are likely to offer a better co-doping effect in the desired C_2 sites as compared to the hydrothermally processed GNR.

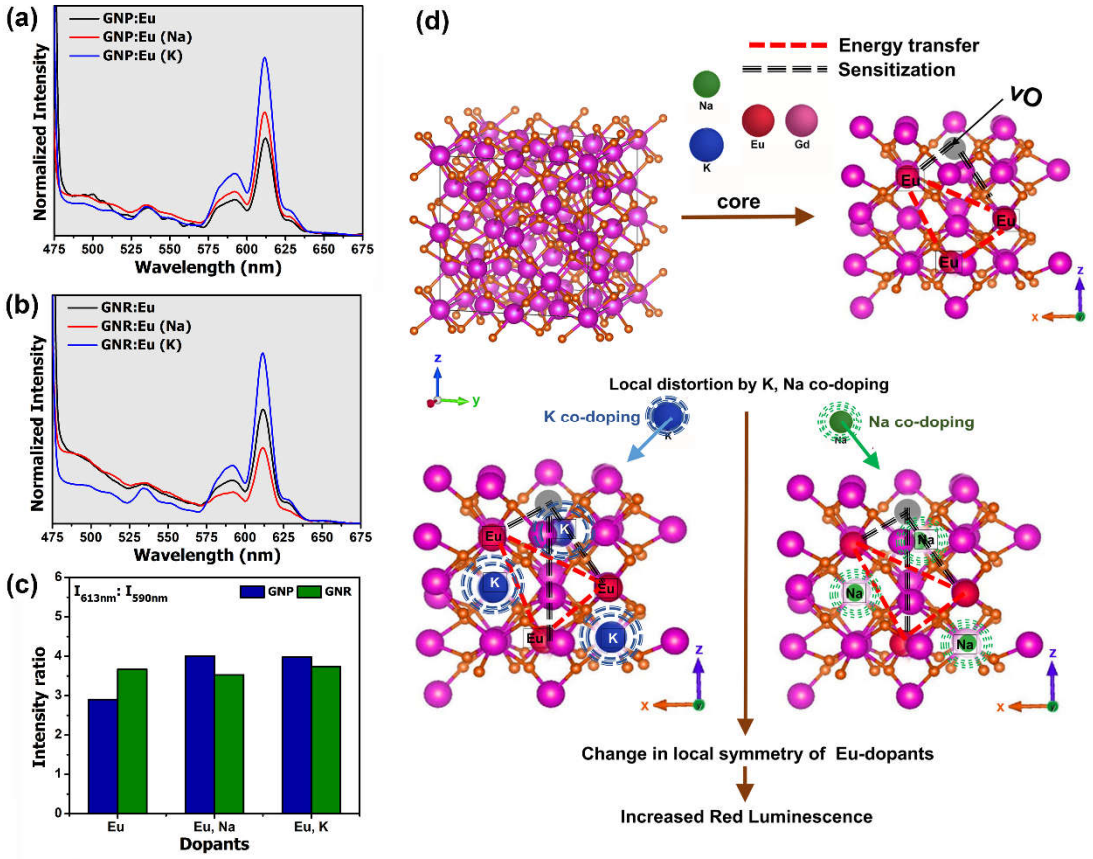

FIGURE 3.11: Normalized PL features without and with co-doping: (a) GNP, and (b) GNR nanosystems. The ED- to- MD transition intensity ratios of the samples are depicted in (c), on a comparative basis. The underlying mechanism in the augmentation of emission process is shown in a scheme, in (d).

Integration of alkali co-dopant metal ions in the host lattice structure generates local stress in the adjacent ions and disturbs the native environment of activator ions. The alkali metal ions substitute for Gd^{3+} in the matrix, which could then aggravate the local symmetry and result in the formation of point defects, mainly oxygen vacancies. These defects can act as sensitizer and facilitate transfer of energy between the host Gd^{3+} and Eu^{3+} ions. Such a strong mixing of charge-transfer states can eventually lead to augmentation in the emission profiles depending on their ionic radii and type of co-dopants affect local structural ordering [46]. While some ions act as sensitizers, others enter into the host lattice which promotes creation of oxygen vacancies,

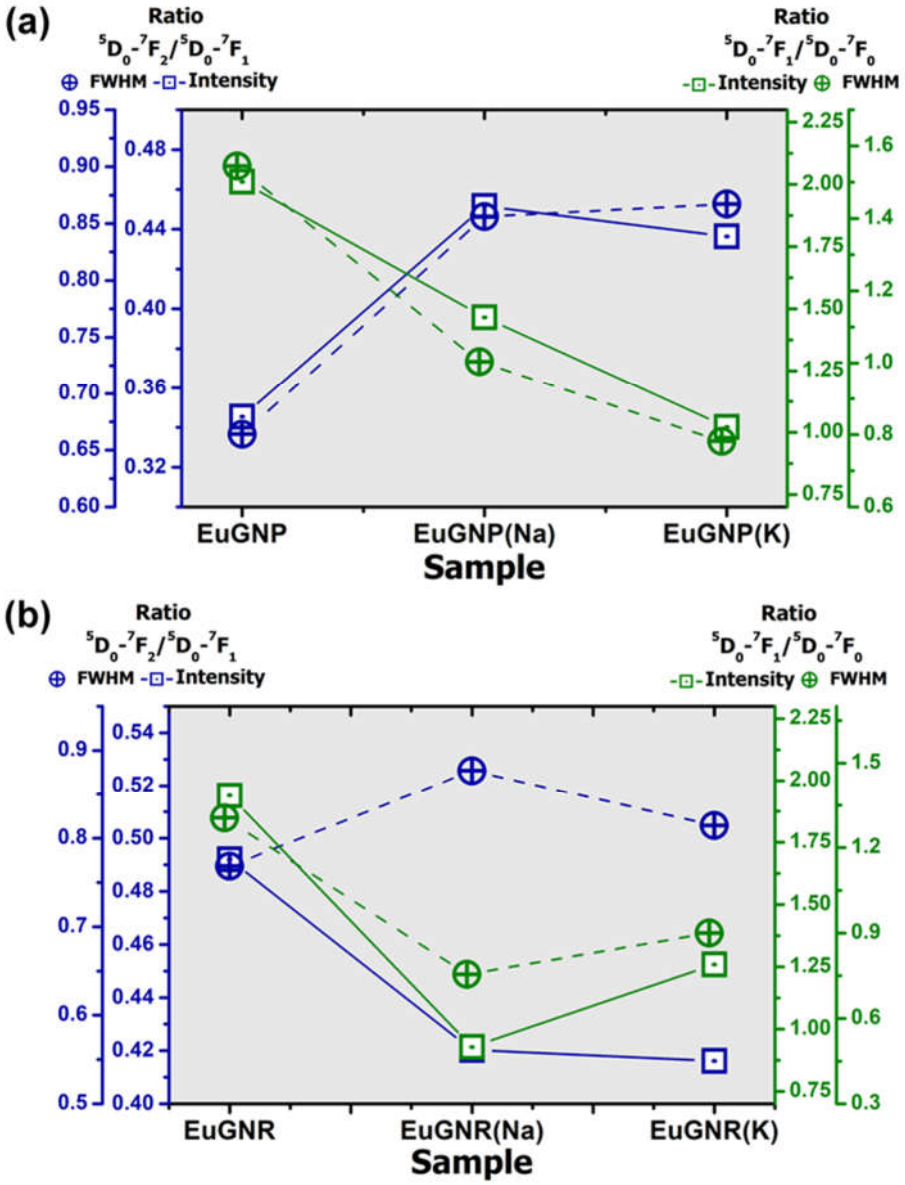

FIGURE 3.12: Comparison of the selective transitional intensities and FWHM ratios for the emission peaks located at ~626 nm ($^5D_0$-$^7F_2$), ~590 nm ($^5D_0$-$^7F_1$) and ~580 nm ($^5D_0$-$^7F_0$) for (a) GNP, and (b) GNR nanosystems.

primarily realized in oxide compounds [47, 48]. The co-dopants may also alter the crystal field due to the host matrix adjoining the activator ions, thus affecting their phosphorescence [49].

The mismatch in the ionic radii and charge state of M^+ with that of the host RE ions could act as the cause for the introduction of some bound *e-h* pairs. As a consequence of generation of stress, the reduced symmetry alters the crystal field

around the Eu^{3+} ions and improve the possibility of radiative electronic transitions, which leads to a rise in PL emission intensity with lifted parity selection rule [50, 51]. Furthermore, manifestation of lattice defects due to incorporation of co-dopants as revealed by a lowering of crystallinity and thereby the increment in dislocation density, greatly influences the local symmetry of the Eu^{3+} ions. The availability of uneven ionic charges could lead to the enhancement of the local distortion, thereby facilitating ED mediated transitions [52].

Transitions from $^5D_1$ levels are responsible for the occurrence of peaks in the blue green regime. If we observe closely in **FIGURE 3.11**, the peak intensity in the blue green regime has decreased in the case of EuGNR(K). This indicates that there is an increase in population levels in the $^5D_0$ level due to radiationless transitions from higher energy levels like, $^5D_1$, $^5D_2$ to ground $^5D_0$ level, followed by the increase in intensity in the red-regime. Although the emission intensity of EuGNR(Na) drops as compared to that of the EuGNR, it is observed that the intensity ratio of the two major *D-F* transitions (612 nm and 590 nm) is greater in EuGNR system as compared to that of the EuGNP (**FIGURE 3.11** (c). However, the ratio of intensity of the two transitions is maximal in the case of EuGNR(Na) which allows it to be termed as a better red phosphor amongst the ones studied. Surprisingly, as for nanorods, the ratios do not increase to a greater extent and lies between ~ 3.5-3.8. While elaborating the results, the variation in ionic radii should also held accountable. Knowing that the ionic radius of K^+ is 1.33 Å and that of Na^+ is 0.97 Å, the variation upsurges the range of available sub-lattice structure around the activators, thereby stimulating the spin-orbit coupling and also disturbs the crystal field effect on Eu^{3+} ions [53, 54]. Creation of some bound electron-hole (e-h) pairs due to incorporation of metal alkali atoms in the host can also be anticipated.

3.4.2. Effect of morphology on luminescence response

As shown in **FIGURE 3.10**, most of the nanosystems presented a better PL feature in presence of co-dopants. This can be validated considering presence of surface trap sites that quench the luminescence profiles [55]. The nanorods are formed

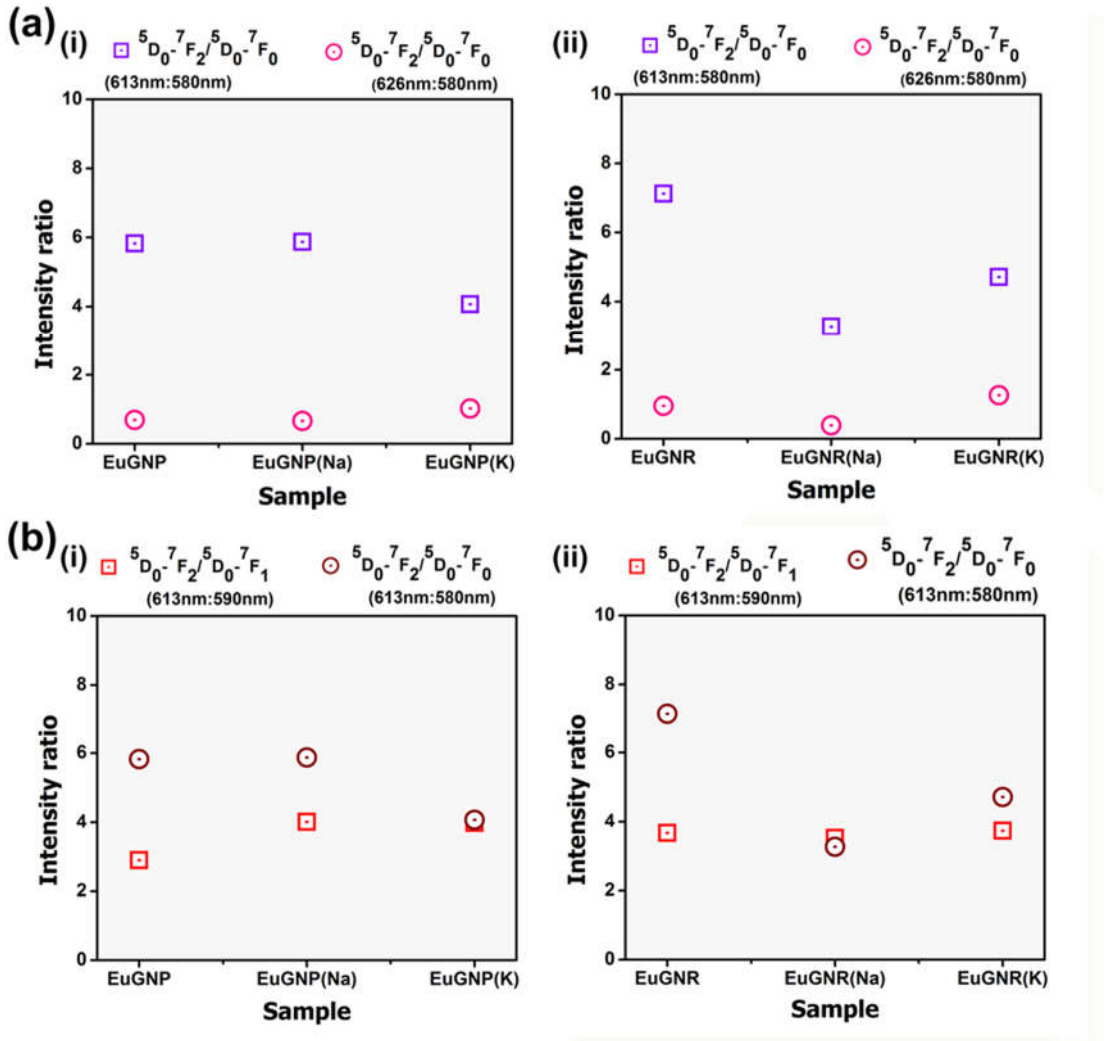

FIGURE 3.13. A comparative account on the PL relative intensity features accompanied via different transitions for the GNP and GNR nanosystems.

due to oriental attachment of nanoparticles and are greater in size as compared to the spherical nanoparticles. It has been reported that the particle size has negligible effect in the *D*→*F* transitions of Eu^{3+} ions considering the intra-*4f* transition mediated emission bands in Eu^{3+} ions [56, 57]. However, smaller sizes imply a larger surface and thus greater number of defects that act as quenchers rather than sensitizing the luminescence response [58, 59]. A decrease in thickness also implies decrement in radiative transition probability due to surface quenching effect resulting in trapped energy of activators by surface defects and other quenching sites present in the surface [60]. As compared to the nanorods (GNR), the nanoparticles (GNP) have greater

surface areas and hence quenching due to near surface sites is prevailed. Surface sites also carry dominant recombination routes, which however can be shifted upon by incorporation of an impurity in the confined structure.

The morphology dependent emission intensity observed in our case can also be corroborated considering the variation in number of particles per unit area facing towards incident light. This tends to alter according to variation in morphological features and thereby the number is different for particles and rods [61]. For RE based activators, the transition induced by dopants can be localized and thereby significant increase in the radiative efficiency of emission can be realized [62]. Non-radiative transitions decrease with an increment in aspect ratio and thus EuGNR system with aspect ratio ~3 displayed a better luminescent behavior as compared to the EuGNP having aspect ratio unity [63]. 1D nanostructures can also display lower *e-h* recombination rate due to a greater mobility of electrons being laterally confined and are guided to move in axial direction [63, 64]**.** Henceforth the photoluminescent behavior of GNRs can be improved upon either by modifying the aspect ratio or by incorporation of dopants/co-dopants [65].

3.4.3. Cause of anomalous trend in EuGNR with Na^+ co-doping

It was a matter of surprise on observing an anomalous trend in the PL emission feature of the EuGNR system with the red-emission not augmented upon co-doping with Na^+. The possible reason can be elaborated considering the reactants used in the hydrothermal route. The route normally involves fixing of pH using NaOH as base and HNO_3 as the acidic component. The acid reduces RE oxides into their nitrate products; upon a maintained pH by addition of NaOH, RE hydroxides are produced with $NaNO_3$ being the possible byproduct in the reaction. Notably, the crystallinity predicted for EuGNR(Na) was compromised as compared to EuGNP(Na) which may imply that incorporation of Na^+ into the lattice is more favored in the latter case. The general reactions for obtaining GNR can be as described below:

$$(\text{Bulk})\ Gd_2O_3 + HNO_3 \rightarrow Gd(NO_3)_3 + 3H_2O,$$

$$Gd(NO_3)_3 + NaOH \rightarrow Gd(OH)_3 + 3NaNO_3,$$

$$Gd(OH)_3 \rightarrow (\text{Nanoscale})\ Gd_2O_3.$$

While for Na^+ co-doping the precursor used is $NaNO_3$, it is highly possible that various sites are already occupied by Na^+ during the preparation of Eu^{3+}:Gd_2O_3 and hence the increment in the 612 nm-to-590 nm ratio as compared to that prepared via the citrate gel route. With the addition of $NaNO_3$ the reaction is compromised with a tendency to go beyond the optimal doping of Na^+ ions, which in turn could not assist further incorporation of Na^+ into the host matrix. The intensity ratio is at par with the EuGNR, and yet more than that of EuGNP. An excess of atoms could also aggregate on the grain boundaries due to a low solubility of alkali atoms in Eu^{3+}:Gd_2O_3 leading to surface states which would affect the surface kinetics. The low level of crystallinity revealed for EuGNR(Na) implies that the synthesis route is not suitable to produce highly crystalline sample and a reasonable amount of unwanted byproduct is attained. Existing literature also suggests that for the $^5D_0 \rightarrow {}^7F_2$ transition in RE based system, the choice of precursors also plays a significant role [56]. On the other hand, an increased shielding of the Eu^{3+} activator ions from quenching collisions in RE acetates can result in an increased asymmetry in Eu^{3+} locality [56]. Such shielding involved in routes with acetate precursors (citrate gel route), can facilitate adequate ligand-ligand exchange between the activator RE species and co-dopant alkali ions which could activate radiative mechanism [66] and consequently, a profound increase in PL intensity has been realised.

3.5. Concluding remarks

The concentration quenching was witnessed at a critical concentration of 3% EuGNP. Our analysis following Dexter's theory led to a stimulating observation due to an exchange interaction of ions. The Effect of overlapping of near zone ED fields of activators hence needs to be further investigated and discussed in detail. For 7% EuGNP nanosystem, a rise in intensity of peaks for $^5D_0 \rightarrow {}^7F$ transitions was observed while intensity for $^5D_1 \rightarrow {}^7F$ transitions decreased. This can be elucidated citing higher doping concentrations favour emission from $^5D_0$ level at the expense of higher excited states related transitions. Following the emission profiles in the blue-green regime, it

can be established that a large number of crystal field transitions influence these levels to follow non-radiative transitions between $^5D_1$ to $^5D_0$. Moreover, the quenching in high energy level emission could be favourable for lower energy emission following multiple cross relaxation events. Profound splitting of ED transitions into non-degenerate and degenerate components was revealed too. Furthermore, the peak for $^7F_3$ were found to split into optically active components. Out of the various transitions via $^5D_0$-^7F_J (J=0,1,2,3,4) in the red and far red regime the $^5D_0$-$^7F_0$ transition, positioned at ~580 nm is a captivating observation confirming *J*-mixing due to crystal field perturbation and/or mixing of low lying charge transfer states into wavefunctions of $^4f_6$ configuration. PL profiling upon temperature variation enabled us to outline the vibronic contribution to the spectra. PL emission profiles of γ-irradiated samples further elate the effect of distorted local field leading to peak splitting. Non-uniform incorporation of dopant ions leads to Eu^{3+} cluster zones and zones barren of Eu^{3+} ion leading to different local field and symmetry induced splitting. To the best of our knowledge, no reports available elaborates the effects of γ-irradiation in the PL response at the blue-green region. Defect formations due to irradiation induced creation of closely packed non-radiative trap centres include both neutral as well as ionized vacancies. Hence, indicating two possible excitation pathways to populate the $^5D_0$ level, one being via $^5D_1$ level and the other promoting ions directly into $^5D_0$ upon higher dose, as the distances between localised entities decrease. Non-radiative relaxation caused by the surface defects acting as quenchers was also observed after irradiation. Moreover, the remarkable 4-fold increment of PL intensity ratio for the ED and MD transition due to the inclusion of the alkali metal ions as co-dopant can be credited to the distortion introduced in crystal field surrounding Eu^{3+} activator.

Bibliography

[1] Clough, R., Nuclear instruments and methods in physics research section B: Beam interactions with materials and atoms. *Nuclear Instruments and Methods in Physics Research, Section B Beam Interactions with Materials and Atoms*, 185(1–4) 8-33, 2001.

[2] Devi, M., Mohanta, D., and Saha, A., Comparative study of microscopic, spectroscopic and magneto-optic response of ferrofluids subjected to γ-radiation. *Indian Journal of Physics*, 89(2) 115-121, 2015.

[3] Tamrakar, R.K., Upadhyay, K., and Bisen, D.P., Gamma ray induced thermoluminescence studies of yttrium (III) oxide nanopowders doped with gadolinium. *Journal of Radiation Research and Applied Sciences,* 7(4) 526-531, 2014.

[4] West, G.A. and Clements, N.S., A comparison of the Eu3+ temperature dependent emission lifetimes in Sc_2O_3, Y_2O_3 and Gd_2O_3 host crystals. *Journal of Luminescence*, 54(4) 245-248, 1992.

[5] Singh, A., O'Donnell, K., Edwards, P., Cameron, D., Lorenz, K., Kappers, M., Boćkowski, M., Yamaga, M., and Prakash, R., Luminescence of Eu^{3+} in GaN (Mg, Eu): Transitions from the $^5D_1$ level. *Applied Physics Letters*, 111(24) 241105, 2017.

[6] Forcales, M., Klik, M., Vinh, N., Bradley, I., Wells, J.R., and Gregorkiewicz, T., Free-electron laser studies of energy transfer mechanisms in semiconductors doped with transition series ions. *Journal of Luminescence*, 94 243-248, 2001.

[7] Zatsepin, A., Kuznetsova, Y., Spallino, L., Pustovarov, V., and Rychkov, V., Photosensitive defects in Gd_2O_3–advanced material for solar energy conversion. *Energy Procedia*, 102 144-151, 2016.

[8] Kang, Y.C., Park, S., Lenggoro, I., and Okuyama, K., Gd_2O_3:Eu phosphor particles with sphericity, submicron size and non-aggregation characteristics. *Journal of Physics and Chemistry of Solids*, 60(3) 379-384, 1999.

[9] Binnemans, K., Interpretation of europium (III) spectra. *Coordination Chemistry Reviews*, 295 1-45, 2015.

[10] Takahei, K., Taguchi, A., Nakagome, H., Uwai, K., and Whitney, P., Intra-4f-shell luminescence excitation and quenching mechanism of Yb in InP. *Journal of Applied Physics*, 66(10) 4941-4945, 1989.

[11] Binnemans, K. and Görller-Walrand, C., Application of the Eu^{3+} ion site symmetry determination. *Journal of Rare Earths*, 14 173, 1996.

[12] Chen, X. and Liu, G., The standard and anomalous crystal-field spectra of Eu^{3+}. *Journal of Solid State Chemistry*, 178(2) 419-428, 2005.

[13] Porcher, P. and Caro, P., Influence of J-mixing on the phenomenological interpretation of the Eu^{3+} ion spectroscopic properties. *Journal of Luminescence*, 21(2) 207-216, 1980.

[14] Tanaka, M., Nishimura, G., and Kushida, T., Contribution of J mixing to the $^5D_0 - ^7F_0$ transition of Eu^{3+} ions in several host matrices. *Physical Review B*,49(24) 16917, 1994.

[15] Malta, O., Lanthanide f↔f transitions hypersensitive to the environment. *Molecular Physics*, 42(1) 65-72, 1981.

[16] Li, G., Lai, Y., Cui, T., Yu, H., Liu, D., and Gan, S., Luminescence properties and charge compensation of $Sr_3Al_2O_6$ doped with Ce^{3+} and alkali metal ions. Materials Chemistry and Physics, 124(2-3) 1094-1099, 2010.

[17] Wang, G., Wang, Z., Zhang, Y., Fei, G., and Zhang, L., Controlled synthesis and characterization of large-scale, uniform Dy $(OH)_3$ and Dy_2O_3 single-crystal nanorods by a hydrothermal method. *Nanotechnology*, 15(9) 1307, 2004.

[18] Blasse, G. and Grabmaier, B., A general introduction to luminescent materials, in *Luminescent materials*. Springer, 1-9, 1994.

[19] Riwotzki, K. and Haase, M., Wet-chemical synthesis of doped colloidal nanoparticles: YVO:Ln (Ln= Eu, Sm, Dy). *The Journal of Physical Chemistry B*, 102(50) 10129-10135, 1998.

[20] Wright, A.O., Seltzer, M.D., Gruber, J.B., and Chai, B.H., Site-selective spectroscopy and determination of energy levels in Eu^{3+}-doped strontium fluorophosphate. *Journal of Applied Physics*, 78(4) 2456-2467, 1995.

[21] Bünzli, J.-C.G., Lanthanide luminescence: from a mystery to rationalization, understanding, and applications, in *Handbook on the Physics and Chemistry of Rare Earths*. Elsevier, 141-176, 2016.

[22] Horrocks, W.D. and Sudnick, D.R., Time-resolved europium (III) excitation spectroscopy: a luminescence probe of metal ion binding sites. *Science*, 206(4423) 1194-1196, 1979.

[23] Smith, E.R., Gruber, J.B., Wellenius, P., Muth, J.F., and Everitt, H.O., Spectra and energy levels of Eu^{3+} in cubic phase Gd_2O_3. *Physica Status Solidi* (b), 247(7) 1807-1813, 2010.

[24] Macedo, A.G., Ferreira, R.A., Ananias, D., Reis, M.S., Amaral, V.S., Carlos, L.D., and Rocha, J., Effects of phonon confinement on anomalous thermalization, energy transfer, and upconversion in Ln^{3+}-doped Gd_2O_3 nanotubes. *Advanced Functional Materials*, 20(4) 624-634, 2010.

[25] Raju, G.S.R., Pavitra, E., and Yu, J.S., Facile template free synthesis of $Gd_2O(CO_3)_2 \cdot H_2O$ chrysanthemum-like nanoflowers and luminescence properties of corresponding Gd_2O_3:RE^{3+} spheres. *Dalton Transactions*, 42(32) 11400-11410, 2013.

[26] Buijs, M., Meyerink, A., and Blasse, G., Energy transfer between Eu^{3+} ions in a lattice with two different crystallographic sites: Y_2O_3:Eu^{3+}, Gd_2O_3: Eu^{3+} and Eu_2O_3. *Journal of Luminescence*, 37(1) 9-20, 1987.

[27] Garcıa-Murillo, A., Le Luyer, C., Dujardin, C., Martin, T., Garapon, C., Pedrini, C., and Mugnier, J., Elaboration and scintillation properties of Eu^{3+}-doped Gd_2O_3 and Lu_2O_3 sol–gel films. *Nuclear Instruments and Methods in Physics Research Section A: Accelerators, Spectrometers, Detectors and Associated Equipment*, 486(1-2) 181-185, 2002.

[28] Blasse, G., Bril, A., and Nieuwpoort, W., On the Eu^{3+} fluorescence in mixed metal oxides: Part I—The crystal structure sensitivity of thr intensity ratio of electric and magnetic dipole emission. *Journal of Physics and Chemistry of Solids*, 27(10) 1587-1592, 1966.

[29] O'Donnell, K., Edwards, P., Yamaga, M., Lorenz, K., Kappers, M., and Boćkowski, M., Crystalfield symmetries of luminescent Eu^{3+} centers in GaN: The importance of the $^5D_0$ to $^7F_1$ transition. *Applied Physics Letters*, 108(2) 022102, 2016.

[30] Bünzli, J.-C.G. and Eliseeva, S.V., Basics of lanthanide photophysics, in *Lanthanide Luminescence*. Springer, 1-45, 2010.

[31] Brecher, C., Samelson, H., Lempicki, A., Riley, R., and Peters, T., Polarized Spectra and Crystal-Field Parameters of Eu^{3+} in YVO_4. *Physical Review*, 155(2) 178, 1967.

[32] Binnemans, K. and Moors, D., Narrow band photoluminescence of europium-doped liquid crystals. *Journal of Materials Chemistry*, 12(12) 3374-3376, 2002.

[33] Bünzli, J.-C.G., Moret, E., Foiret, V., Schenk, K.J., Mingzhao, W., and Linpei, J., Structural and photophysical properties of europium (III) mixed complexes with β-diketonates and o-phenanthroline. *Journal of Alloys and Compounds*, 207 107-111, 1994.

[34] Tsai, B.-S., Chang, Y.-H., and Chen, Y.-C., Nanostructured red-emitting $MgGa_2O_4$:Eu^{3+} phosphors. *Journal of Materials Research*, 19(5) 1504-1508, 2004.

[35] Dexter, D.L. and Schulman, J.H., Theory of concentration quenching in inorganic phosphors. *The Journal of Chemical Physics*, 22(6) 1063-1070, 1954.

[36] Pang, M., Lin, J., and Yu, M., Fabrication and luminescent properties of rare earths-doped $Gd_2(WO_4)_3$ thin film phosphors by Pechini sol–gel process. *Journal of Solid State Chemistry*, 177(7) 2237-2241, 2004.

[37] Blasse, G., Energy transfer in oxidic phosphors. *Philips Research Reports*, 24(2) 131, 1969.

[38] Pang, M., Lin, J., Fu, J., Xing, R., Luo, C., and Han, Y., Preparation, patterning and luminescent properties of nanocrystalline Gd_2O_3:A (A= Eu^{3+}, Dy^{3+}, Sm^{3+}, Er^{3+}) phosphor films via Pechini sol–gel soft lithography. *Optical Materials*, 23(3-4) 547-558, 2003.

[39] Fang, T.-H., Hsiao, Y.-J., Chang, Y.-S., and Chang, Y.-H., Photoluminescent characterization of $KNbO_3$:Eu^{3+}. *Materials Chemistry and Physics*, 100(2-3) 418-422, 2006.

[40] Dexter, D.L., A theory of sensitized luminescence in solids. *The Journal of Chemical Physics*, 21(5) 836-850, 1953.

[41] Van Uitert, L., Characterization of energy transfer interactions between rare earth ions. *Journal of the Electrochemical Society*, 114(10) 1048-1053, 1967.

[42] Birgeneau, R., Hutchings, M., and Wolf, W., Temperature Variation and Separation Dependence of Exchange Interactions of Gd^{3+} Pairs in $LaCl_3$. *Physical Review Letters*, 17(6) 308, 1966.

[43] Rao, D., Tovar, M., Oseroff, S., Vier, D., Schultz, S., Thompson, J., Cheong, S.W., and Fisk, Z., Crystal-field and exchange interactions of dilute Gd^{3+} ions in Eu_2CuO_4. Physical Review B, 38(13) 8920, 1988.

[44] Ozawa, L., Forest, H., Jaffe, P., and Ban, G., The effect of exciting wavelength on optimum activator concentration. *Journal of the Electrochemical Society*, 118(3) 482-486, 1971.

[45] Blasse, G., Influence of local charge compensation on site occupation and luminescence of apatites. *Journal of Solid State Chemistry*, 14(2) 181-184, 1975.

[46] Jeong, J.H., Yang, H.K., Shim, K.S., Jeong, Y.R., Moon, B.K., Choi, B.C., Bae, J.S., Yi, S.S., and Kim, J.H., Li doping effect on the luminescent characteristics of YVO_4:Eu^{3+} thin films grown by pulsed laser deposition. *Applied Surface Science*, 253(19) 8273-8277, 2007.

[47] Yi, S.-s., Bae, J.S., Shim, K.S., Jeong, J.H., Park, J.-C., and Holloway, P., Enhanced luminescence of Gd_2O_3:Eu^{3+} thin-film phosphors by Li doping. *Applied Physics Letters*, 84(3) 353-355, 2004.

[48] Chi, L., Liu, R., and Lee, B., Synthesis of Y2O3: Eu, Bi red phosphors by homogeneous coprecipitation and their photoluminescence behaviors. *Journal of the Electrochemical Society*, 152(8) J93-J98, 2005.

[49] Liu, X., Han, K., Gu, M., Xiao, L., Ni, C., Huang, S., and Liu, B., Effect of codopants on enhanced luminescence of $GdTaO_4:Eu^{3+}$ phosphors. *Solid State Communications*, 142(12) 680-684, 2007.

[50] Macfarlane, R. and Shelby, R., *Spectroscopy of solids containing rare earth ions.* edited by AA Kaplyanskii and R. Macfarlane, North-Holland, Amsterdam, 1987.

[51] Waldrip, K., Lewis, J., Zhai, Q., Puga-Lambers, M., Davidson, M., Holloway, P., and Sun, S.-S., Improved electroluminescence of ZnS: Mn thin films by codoping with potassium chloride. *Journal of Applied Physics*, 89(3) 1664-1670, 2001.

[52] Mukherjee, S., Dasgupta, P., and Jana, P.K., Size-dependent dielectric behaviour of magnetic Gd2O3 nanocrystals dispersed in a silica matrix. *Journal of Physics D: Applied Physics*, 41(21) 215004, 2008.

[53] Shi, S., Gao, J., and Zhou, J., Effects of charge compensation on the luminescence behavior of Eu^{3+} activated $CaWO_4$ phosphor. *Optical Materials*, 30(10) 1616-1620, 2008.

[54] Dhananjaya, N., Nagabhushana, H., Nagabhushana, B., Rudraswamy, B., Shivakumara, C., Narahari, K., and Chakradhar, R., Enhanced photoluminescence of $Gd_2O_3:Eu^{3+}$ nanophosphors with alkali (M= Li+, Na+, K+) metal ion co-doping. *Spectrochimica Acta Part A: Molecular and Biomolecular Spectroscopy*, 86 8-14, 2012.

[55] Wang, X., Xu, J., Yu, J., Bu, Y., Marques-Hueso, J., and Yan, X., Morphology control, spectrum modification and extended optical applications of rare earth ion doped phosphors. *Physical Chemistry Chemical Physics*, 22(27) 15120-15162, 2020.

[56] Sharma, P. K., Jilavi, M. H., Nass, R., & Schmidt, H. Tailoring the particle size from μm→ nm scale by using a surface modifier and their size effect on the fluorescence properties of europium doped yttria. *Journal of Luminescence*, 82(3), 187-193, 1999.

[57] Leng, Z., Zhang, N., Liu, Y., Li, L., and Gan, S., Controlled synthesis of different multilayer architectures of $GdBO_3:Eu^{3+}$ phosphors and shape-dependent luminescence properties. *Applied Surface Science*, 330 270-279, 2015.

[58] Yang, L., Zhou, L., Huang, Y., and Tang, Z., Controlled synthesis of different morphologies of $GdBO_3$:Eu^{3+} crystals and shape-dependent luminescence properties. *Materials Chemistry and Physics*, 131(1-2) 477-484, 2011.

[59] Shao, B., Zhao, Q., Guo, N., Jia, Y., Lv, W., Jiao, M., Lü, W., and You, H., Monodisperse YVO_4: Eu^{3+} submicrocrystals: controlled synthesis and luminescence properties. *CrystEngComm*, 15(29) 5776-5783, 2013.

[60] Wang, F., Wang, J., and Liu, X., Direct evidence of a surface quenching effect on size-dependent luminescence of upconversion nanoparticles. *Angewandte Chemie International Edition*, 49(41) 7456-7460, 2010.

[61] Sharma, P.K., Jilavi, M., Burgard, D., Nass, R., and Schmidt, H., Hydrothermal Synthesis of Nanosize alpha-Al_2O_3 from Seeded Aluminum Hydroxide. *Journal of the American Ceramic Society*, 81(10) 2732-2734, 1998.

[62] Bhargava, R., The role of impurity in doped nanocrystals. *Journal of Luminescence*, 72 46-48, 1997.

[63] Yang, E., Li, G., Fu, C., Zheng, J., Huang, X., Xu, W., and Li, L., Eu^{3+}-doped Y_2O_3 hexagonal prisms: shape-controlled synthesis and tailored luminescence properties. *Journal of Alloys and Compounds*, 647 648-659, 2015.

[64] Wang, Z., Wu, L., Zhou, J., Cai, W., Shen, B., and Jiang, Z., Magnetite nanocrystals on multiwalled carbon nanotubes as a synergistic microwave absorber. *The Journal of Physical Chemistry C*, 117(10) 5446-5452, 2013.

[65] Chall, S., Mati, S.S., Rakshit, S., and Bhattacharya, S.C., Soft-templated room temperature fabrication of nanoscale lanthanum phosphate: synthesis, photoluminescence, and energy-transfer behavior. *The Journal of Physical Chemistry C*, 117(47) 25146-25159, 2013.

[66] Matthews, L.R., Wang, X.-j., and Knobbe, E., Concentration effects on the luminiscence behavior of europium (III) chloride-and organoeuropium-doped silicate gels. *Journal of Non-Crystalline Solids*, 178 44-51, 1994.